Investigation of Waveguides and Optical Fibres

PHY3007 Optics Project

Luke Devlin 40356759

School of Mathematics and Physics
Queen's University Belfast
United Kingdom
11th April 2025

Abstract

This report presents an experimental investigation into the behaviour and performance of optical waveguides and fibre optic components under varying conditions. Key aspects explored include light propagation through dielectric interfaces, total internal reflection, attenuation, dispersion, and the impact of source characteristics on transmission quality. Both laser diodes and LEDs were analysed over fibre lengths ranging from 1m to 100km, with transmission performance evaluated via eye diagrams, Q-factor measurements, and Bit Error Rate (BER) analysis.

Results demonstrate that laser sources yield significantly higher signal integrity over short distances, while longer fibre links at higher bit rates suffer from inter-symbol interference and increased BER due to dispersion and power loss. Fibre Bragg Gratings (FBGs) showed clear temperature-dependent wavelength shifts, confirming their value in sensing applications. Dense Wavelength Division Multiplexing (DWDM) filters centred at ITU channels 34 and 35 exhibited excellent spectral selectivity and isolation, while the impact of controlled optical attenuation was quantified using a Variable Optical Attenuator (VOA).

Overall, the study validates core principles of optical waveguiding and highlights the performance trade-offs involved in designing efficient fibre optic communication systems.

Introduction

The rapid growth of global data traffic has made the use of optical fibres and optical waveguides evermore prevalent in modern society and the use of waveguiding can be see everywhere from data transmission to advancements in biomedical engineering [1]. The main premise of this report is to bring together the seminal work which has been done in the field of optical fibre communications and to highlight the technological advances which have allowed us to achieve rates of digital information transfer of up to 402 Tb/s according to the most recent research. [2] The overall scope of the report is to gain a better understanding of the current developments of optical fibres and to verify the physical concepts which are used to help create this technology. This is done by investigating the fundamental and practical aspects of optical waveguiding, the reliability of data transmission via Bit Error Rate (BER) analysis, and the characterization of key WDM components, providing valuable insight into the design of modern photonic networks. These technologies are essential in high-speed communication systems due to their low loss and high bandwidth capabilities

Reflection And Refraction

Snell's Law and Fresnel's Equations

The investigation into waveguides begins with verifying the some of the core physics which quantifies the propagation of light from one medium to another; Snell's Law and Fresnel's Equations.

$$\boxed{n_i \sin\theta_i = n_t \sin\theta_t}$$

$$\boxed{R_i = \left(\frac{n_t \cos\theta_i - n_i \cos\theta_t}{n_i \cos\theta_t + n_t \cos\theta_i}\right)^2}$$

$$\boxed{R_o = \left(\frac{n_i \cos\theta_i - n_t \cos\theta_t}{n_i \cos\theta_i + n_t \cos\theta_t}\right)^2}$$

Where

- n_i is the refractive index of the incident medium (where the light originates).
- n_t is the refractive index of the transmission medium (into which the light enters).
- θ_i is the angle of incidence, measured from the normal to the interface.
- θ_t is the angle of transmission (or refraction), also measured from the normal, determined using Snell's Law.
- R_i is the Fresnel reflection coefficient for p-polarized (parallel) light, representing the fraction of power reflected.
- R_o is the Fresnel reflection coefficient for s-polarized (perpendicular) light, representing the fraction of power reflected.

Both of these equations give us insight into the properties of how light changes when moving from one medium to another. The amplitude of the reflected and transmitted light is characterised by the incident angle θ_i, the polarisation state and the refractive indices according to Fresnel's Equations; Snell's Law gives us insight into how much the ray of light refracts at the interface of the differing mediums. Both of these equations can be derived from Maxwell's Equations which form the cornerstone of Electromagnetic Theory but the derivations have been omitted from this report and can be found in David Griffiths' "Introduction to Electrodynamics" [3]. The relationship between Brewster's angle and the refractive index can also be shown to be,

$$\boxed{\theta_B = \arctan\left(\frac{n_2}{n_1}\right)}$$

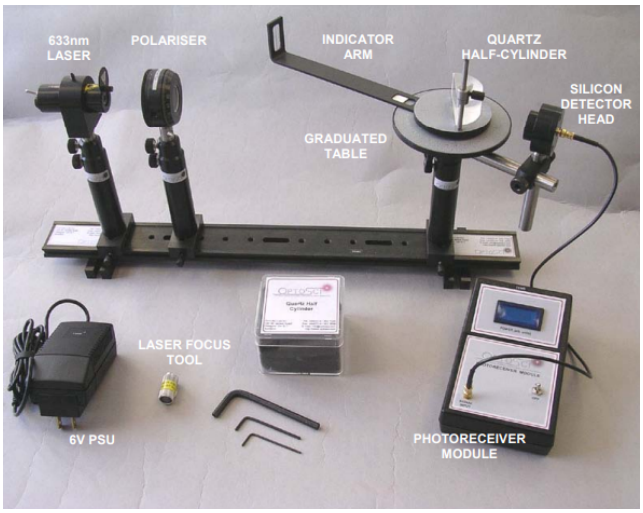

Figure 1: Validating Snell's Law

Results and Analysis

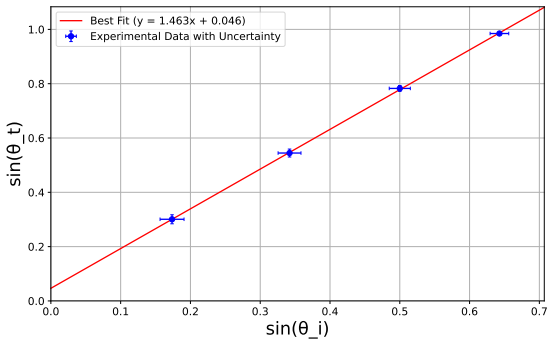

Figure 2: Validating Snell's Law

Our experiments commenced with the following apparatus which is depicted in Figure 1; a 633nm LASER which is categorised as a Class 2 LASER deeming it to be eye safe, a silicon detector head which is used to determine the optical power and a quartz half-cylinder to explore the nature of light in low-to-high and high-to-low refractive index transmissions. The LASER will propagate through the half-quartz cylinder and be incident on a plain white piece of card. The measurements for this experiment were also carried out in the dark to increase the accuracy of the readings because parts of the experiment require that no light is observed. We were able to show what the defining characteristics of the waveguide are through our analysis, namely the refractive index and the critical angle.

Experiments were conducted to relate the reflectance and transmittance of the LASER and determine the Brewster's angle of the quartz half-cylinder, the reflectance and transmittance also depend on the polarisation. In this experiment, the polariser to 45° so that the P and S polarisations are equally weighted and determined Brewster's angle. This is the angle of incidence at which light with a certain polarisation is perfectly transmitted through a surface with no reflection and this occurs only for p-polarized light (light parallel to the plane of propagation). The incident ray of unpolarised light will induce vibrations of electric dipoles along its axis which will emit an electromagnetic wave, this is what causes the refracted ray in the medium. The refracted beam will be 90° with respect to the reflected ray which is along the direction of the dipoles axis, therefore the reflected ray will become completely polarised. We determined two different values for Brewster's angle which was derived from low-to-high transmission and high-to-low transmission; the more accurate being low-to-high transmission.

The critical angle is the angle at which the refracted ray is parallel to the surface of the medium and therefore doesn't transmit through the medium, which in this case was $44° \pm 1°$. The uncertainty which is the width of the LASER's beam on the plain white card. The refractive index can then determine from the critical angle by using Snell's Law and this gives a refractive index of $n = 1.44 \pm 0.03$, this can be validated by Brewster's angle for more validity. According to Figure 3, Brewster's angle is $55° \pm 0.5°$, which gives us a value of $n = 1.43 \pm 0.05$ for the refractive index. This is within the range of certainty for the refractive index that was calculated using the critical angle.

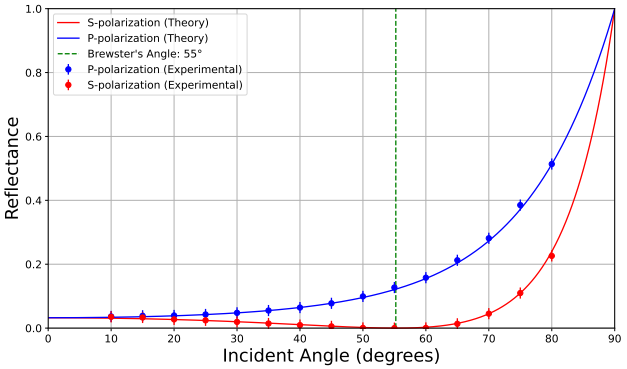

Figure 3: P and S Polarisation High-to-Low

High-to-low transmission was also conducted but was consistently less accurate than low-to-high transmission, this was possibly due to the curved part of the cylinder not being perfectly round and so the LASER is incident at a non-zero angle. For angles which are greater than the critical angle we obtain a constant value for the reflectance which is due to the background electromagnetic radiation.

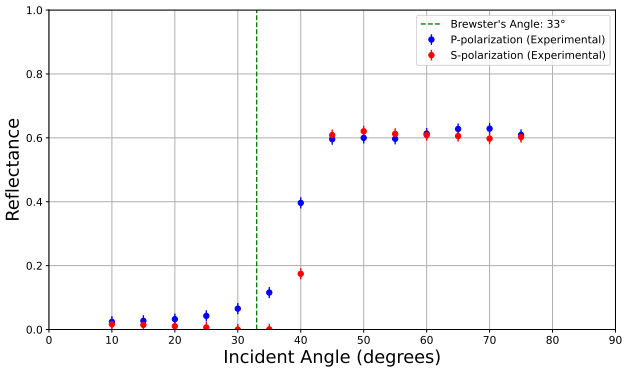

Figure 4: S Polarisation High-to-Low

We can see from Figures 4 what the Brewster's angle is for high-to-low transmission which is $33° \pm 1.54°$. However when using this value of Brewster's angle we get a different refractive index which is $n = 1.54 \pm 0.03$, so we can see just how much more inaccurate the method of measuring the refractive index this way is far less accurate.

Principles of Waveguides

Step and Graded Index Waveguides

The specific objectives of the experiments are; to determine the mode structure of several step index and graded index planar optical waveguides, to measure the number of modes guided and their effective indices for both the TE and TM polarisation states via the prism coupling technique, and to establish designs for the manufacture of single-mode step and graded index planar waveguides. All of which are fundamental to the understanding of light propagation in optical fibres, and to the design of waveguide devices including integrated optical components.

Waveguides are typically made from silica which is doped with germanium dioxide or phosphorus pentoxide to increase their refractive indices, in practise doped waveguides are used to also mitigate the effects of intramodal dispersion (dispersion due to a single-mode). They can also be made from plastics such as PMMA (Polymethyl methacrylate) also known as acrylic, each having their own pros and cons [4]. Glass is less flexible but also has less attenuation loss whereas plastic is more flexible but has a high attenuation loss. Therefore silica waveguides are more used for long distance data transmission whereas the plastic waveguides are more common in short distance transmission.

Step and graded index waveguides are formed by thin film deposition and ion exchange processes respectively. Thin film deposition is a crucial step in the fabrication of step-index optical fibres, where layers of doped and undoped glass are sequentially deposited to form a high-index core and a lower-index cladding to achieve TIR. However, the waveguides that were used for the experiment were fabricated with a different technique, which included spin deposition of a sol-gel solution onto a quartz slide. Spin deposition is the process where a sol-gel solution is pipetted onto a glass substrate and placed onto a disc which rotates at a high speed. In fact, the viscosity at a given speed and will dictate the number of modes the waveguide will have because the viscosity will correlate with the thickness of the sol-gel.

Alternative fabrication methods are used to create graded index fibres. Graded-index fibres are fabricated via thermal diffusion or ion exchange. In the diffusion method, dopants are layered and thermally diffused in a silica preform to produce a desired index profile. In the diffusion process, a layer of material, usually a metal, is vacuum deposited onto a suitable substrate. The structure is then heated in a furnace at a sufficiently high temperature to allow the metal to diffuse into the substrate. The presence of the metal locally increases the refractive index of the material resulting in the creation of the waveguide. The refractive index is greatest at the surface, falling off as we go deeper into the material until it is equal to the index of the substrate. The surface index is determined by the metal thickness, and the waveguide thickness is determined by the diffusion temperature and the diffusion time at that temperature. Waveguides with high diffusion times will have a steeper gradient. In contrast, ion exchange replaces native ions in a glass substrate with larger ions from a molten salt bath, forming a graded profile near the surface. At higher temperatures of the melt, ions in the substrate become mobile and surface ions may exchange with ions from the melt. The surface index is determined by the concentration of the exchange ions in the melt, and the waveguide thickness is defined by the temperature of the melt and the time of immersion. This approach is widely used in planar waveguides and integrated photonic devices due to its simplicity and flexibility.

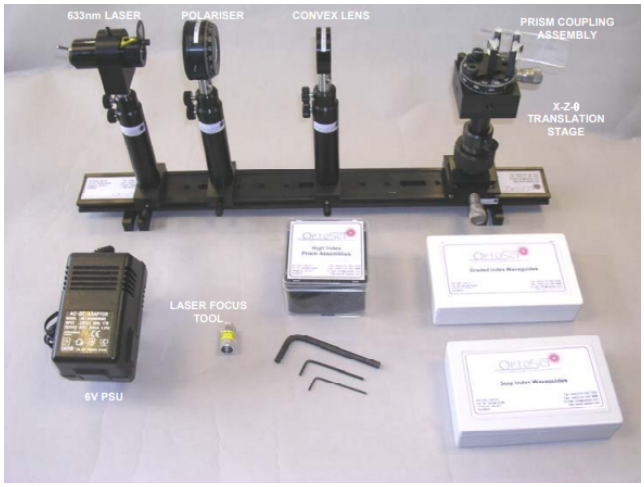

Figure 5: Waveguide Apparatus

The apparatus used for these sets of experiments is similar to that of the previous, wherein the major change is in the implementation of the prism coupling assembly and with the addition of the convex lens as shown in Figure 4.

The method for the experiment consistent of observing the mode lines for various different type of Step and Graded-Index waveguides to compare their thick-

ness and refractive index. The prism coupling assembly turns on its axis and the incident angle of the LASER on the tilted face of the prism can be read. The angle at which these modes appear will give insight into what the refractive index of the substrate is, a derivation is given in the "Prism Coupling" section of the report. Reading were taken for the TE modes, then followed by the TM modes observe the expected change in the refractive indices due to birefringence and to add certainty about the thickness for the waveguide.

Principles of Light Propagation in Waveguides

Light propagates in optical waveguides primarily through the mechanism of total internal reflection (TIR), which forms discrete electromagnetic field distributions known as modes which are showcased in Figure 5. These modes propagate along the axis of the waveguide with a well-defined propagation constant β and a corresponding effective refractive index n_{eff}, such that:

$$\boxed{n_{\text{cladding}} < n_{\text{eff}} < n_{\text{core}}}$$

Only certain field configurations satisfy the boundary conditions, resulting in discrete solutions. These discrete solutions are referred to as guided modes, and each has a distinct spatial field distribution across the waveguide. For example, in a planar waveguide, the supported transverse electric (TE) modes are labelled as TE_0, TE_1, TE_2, et cetera. These modes have an electric field which is totally perpendicular to the direction of propagation and no component of a magnetic field. A transverse magnetic (TM) mode will have a magnetic field which is perpendicular to the direction of propagation but will have some non-zero electric field as well. These modes will partially enter the superstrate air and the substrate quartz of the waveguide and also vary harmonically in the waveguide film. For lower modes the field is highly concentrated at the centre and progressively becomes less concentrated for higher modes until eventually all power is dissipated into the surrounding of the waveguide, this power is radiated out due to the tunnelling effect. We can see how the concentration of the field is spread out more across the waveguide as the mode order increases in figure 3.

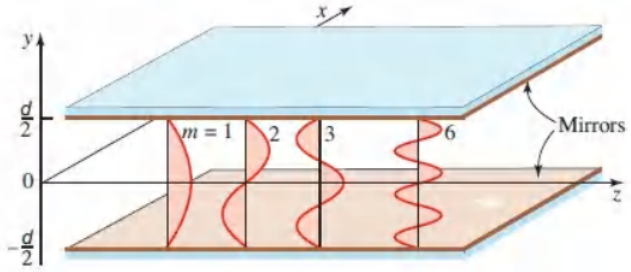

Figure 6: Standing Waveguide Modes [5]

The number of supported modes depends on the waveguide's physical dimensions and the wavelength of light. When only the fundamental mode (typically TE_0) is supported, the waveguide is said to be single-mode. As the waveguide becomes narrower or the wavelength increases, higher-order modes reach a cut-off condition, where their effective index approaches the cladding index and they become unguided. Thus, light in a waveguide propagates as a superposition of these allowed modes, each confined within the core due to total internal reflection and sustained by constructive interference.

Prism Coupling

Prism coupling is an optical technique used to efficiently transmit light into a thin-film planar waveguide, particularly when studying the mode structure of the guide.

In this method, a prism is placed in close proximity to the waveguide surface and a laser beam is directed into the prism at a variable angle. When the incident angle satisfies phase-matching conditions, light from the prism evanescently couples into the waveguide, exciting a guided mode. This coupling occurs because the component of the wavevector along the interface matches the propagation constant of a mode in the waveguide. When light is incident on a planar waveguide through a prism, coupling into guided modes occurs only when the phase-matching condition is satisfied. This condition ensures that the component of the incident wavevector parallel to the waveguide surface matches the propagation constant β of a guided mode.

The wavevector of the light in the prism is:

$$\vec{k}_p = k_0 n_p$$

where:

- $k_0 = \dfrac{2\pi}{\lambda}$ is the free-space wave number,
- n_p is the refractive index of the prism,
- λ is the wavelength of light in vacuum.

The component of this wavevector parallel to the waveguide surface is:

$$k_{\parallel} = k_0 n_p \sin\theta$$

To couple into a mode, this must equal the propagation constant β of that mode:

$$\beta = k_0 n_{\text{eff}}$$

Therefore, the phase-matching condition is:

$$k_0 n_{\text{eff}} = k_0 n_p \sin\theta$$

Cancelling k_0 from both sides gives:

$$n_{\text{eff}} = n_p \sin\theta$$

This effective refractive index can be deduced from the angle of incidence at which the m-lines appear. The direct equation that we use must include the angle of incidence on the prism but the angle θ here is the angle of the incident ray which is normal to the interface between the waveguide film and the prism. To derive the

measurable incident angle we can refer to Figure 6 and use some simple geometry.

Using Snell's Law we can rewrite θ_t as

$$\theta_t = \arcsin(\frac{sin\theta_i}{n_p})$$

and we know

$$\theta_p = A + \theta_t$$

Here θ_p is the same as θ, therefore we can write

$$\boxed{n_{eff} = n_p sin(A + \arcsin(\frac{sin\theta_i}{n_p}))}$$

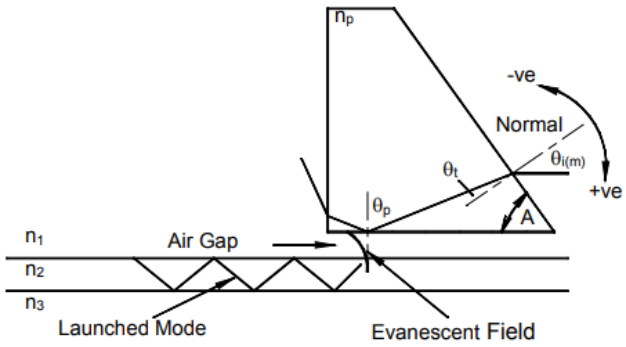

Figure 7: Prism Coupling

Now that we have determined the effective refractive index of the waveguide modes we can plot the different modes for a range of n_2 and we can determine the thickness of the waveguide and its refractive index.

Results and Analysis

Figure 11 is a visual representation of the modes for high Step-Index waveguide, and it is clear to see that there are indeed many modes. Table 1 along with Figure 10 show the effect of birefringence when travelling through the step-index waveguide and is more pronounced at thinner waveguides because the evanescent fields extend more into the substrate and superstrate. Figure 10 shows the change in the propagation constant ($\Delta\beta$) for the two different modes and Table 1 confirms this notion due to the difference of the refractive index for each mode. The thickness and refractive index of the waveguide was found by taking the intersection points between the fundamental mode and the other modes, and the is taken as the midpoint between the intersection of the fundamental mode and the first mode and the fundamental mode and the third mode. This analysis gives a value for $d = 65.2\mu m \pm 6.25\mu m$ and $n = 1.61 \pm 0.004$ for the high step-index waveguide.

Table 1: Table Showing Different Refractive Indices for TE and TM Modes

Mode Number	TE Mode Effective Refractive Index	TM Mode Effective Refractive Index
3	1.564 ± 0.002	1.570 ± 0.002
2	1.573 ± 0.001	1.578 ± 0.002
1	1.587 ± 0.002	1.593 ± 0.003
0	1.602 ± 0.002	1.614 ± 0.004

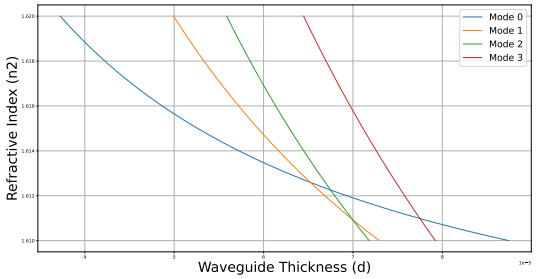

Figure 8: Graph Showing all TE Modes for High Step-Index Waveguide

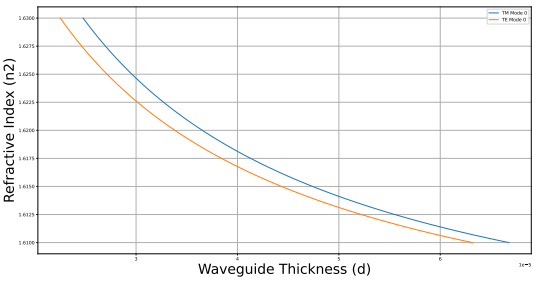

Figure 9: Comparison of TE and TE Fundamental Modes for Low Step-Index Waveguide

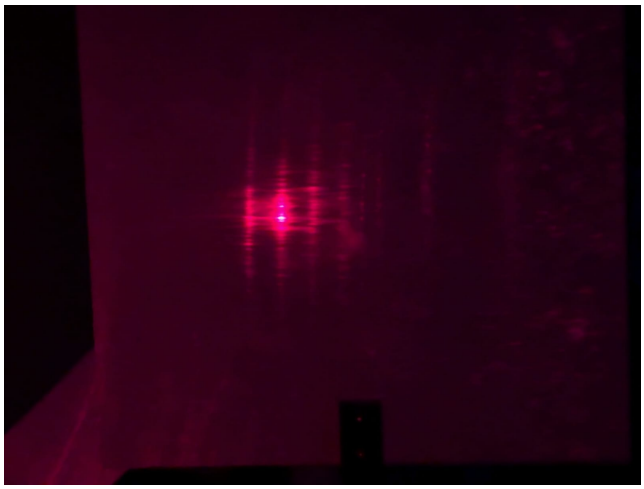

Figure 10: Comparison of TE and TE Fundamental modes

Figure 12 show the modes for a Graded-Index waveguide which was submerged for 18 minutes at 317C and by carrying out a similar analysis for the Graded-

Index waveguides we can determine the same parameters. The waveguide thickness was determined to be $3.177\mu m \pm 0.25\mu m$ and the refractive index was 1.550 ± 0.001. It was also shown that overall the refractive index is smaller in the Graded-index waveguides than the Step-Index waveguides, this is because of less intermodal dispersion occurring the Graded-Index waveguide.

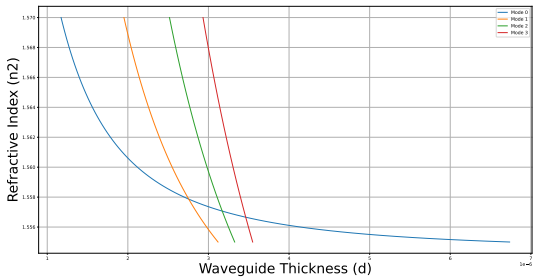

Figure 11: TE Modes for Graded-Index Waveguide

When carrying out this experiment, it is vital to ensure that the waveguides are exceptionally clean and do not have fingerprints present at all. This was the main limited factor when attempting to observe the waveguide modes as the evanescent wave must be fit to penetrate through thickness on the order of 5 to $10\mu m$.

Optical Fibre Communication

Brief History of Optical Fibre Communications

The development of optical fibre communications has been one of the most paramount technological strides in the modern era and its progress spans several decades long. Most of the major progressions in telecommunications has come from breakthroughs in physics and material science. The discovery of LASER technology by Thomas Maiman in his paper "Stimulated Optical Radiation in Ruby" [6] was the very beginning of modern telecommunications as it allows the transfer of information via light. Data transmission can also be achieved via LED however this technique is only used for short distance transmission due to the relatively higher amounts of dispersion and attenuation. LASER is more ubiquitous as it has a sharper spectrum, is more coherent and has higher power output. In 1966, Charles Kao and George Hockham proposed that glass fibres with attenuation below 20 dB/km could be used for long-distance communication [7]. This prediction earned Kao the 2009 Nobel Prize in Physics [8]. Rapid advances in semiconductor lasers, photodetectors, and fibre fabrication led to the deployment of optical fibre systems for telephone and data networks and losses were further reduced to 0.2 dB/km at 1550nm [9]. The introduction of WDM and DWDM systems allowed multiple channels in the same fibre and Erbium-Doped Fibre Amplifiers (EDFAs) enabled long-haul transmission [10]. Currently the leading research in optical fibre communication is in the development of orbital angular momentum (OAM) Multiplexing [11].

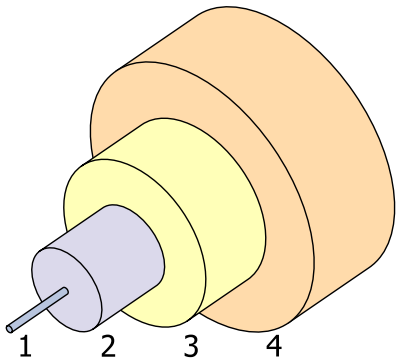

Figure 12: Design of Optical Fibre

- 1.- Core 8-10 µm
- 2.- Cladding 125 µm
- 3.- Buffer 250 µm
- 4.- Jacket 400 µm [12]

Optical Detection Link: Sources and Detectors

The original data is converted into a light source via a transmitter and then propagates through the optical fibre until the light reaches a receiver and is converted back into an electrical signal. The light can be propagated through the fibre with two different sources, an LED or a LASER. The primary characteristics of LASER satisfy the requirements imposed by attenuation to be a better candidate for long distance signal transfer. These characteristics include, but are not limited to significant launch power, a sharp spectrum, high efficiency, emit coherent light and higher bit rates. LED are not used because they have characteristics which are undesirable for high rate data transmission such as a large linewidth, low efficiency, high dispersion and they exhibit decoherence. The characteristics of LEDs and LASERs will be discussed more thoroughly in the results section.

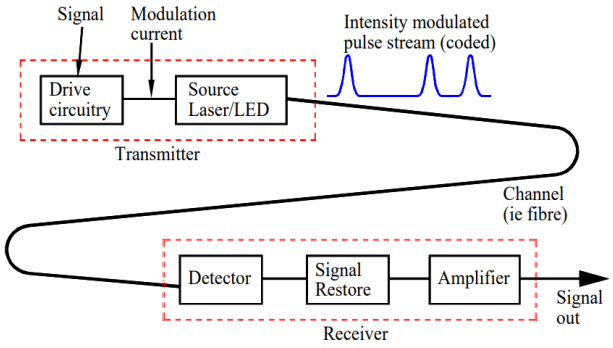

Figure 13: Schematic of a Point to Point Fibre Optic Communications Link [13]

Another crucially important component in the optical fibre channel is the use of photodiodes. Photodiodes are an electrical component which are used to detect

the light signal at the end of the fibre channel. Their sensitivity plays a vital role in the attenuation of the signal and there are many different types of photodiodes which are used to achieve a lower attenuation.

Photodiodes are used to convert a light signal into an electrical current so that the coded stream can be properly interpreted. The working principle behind photodiodes is the photoelectric effect and the use of semiconductors. Whenever photons have a higher energy than the energy band gap are incident on the depletion region of the photodiodes, electron-hole pairs are generated and will be swept by the electric field to produce current.There are some parameters to be made aware of when discussing photodetectors, quantum efficiency being one of the main ones. Quantum efficiency is essentially a quantifiable measurement of how well the photo diode converts light into electrical current. The quantum efficiency (η) of a photodiode is defined as the ratio of the number of carriers generated per second (Ip/q) to the number of incident photons per second (P_o/hv).

$$\boxed{\eta = \frac{I_p hv}{P_o q}}$$

$$\boxed{I_o = \frac{hv}{\eta q} P_o}$$

Reverse biasing is used in a photodiode to increase the depletion region and the strength of the electric field but the effect of reverse biasing is different for the different variants of photodiodes. There are three different types of photodiodes which are commonly used in industry; a PN diode, a PIN diode and an APD diode. Standard PN photodiodes have a simple P-N junction and have limited bandwidth and sensitivity so they are not often used in high-speed fibre optic systems. PIN diode has a different structure in comparison to PN photodiodes. PIN diodes have an intrinsic layer between the P-type and N-type layers, this intrinsic layer increases the width of the depletion region. The intrinsic layer improves the quantum efficiency as more light is absorbed and increases the response time of the diode. The Avalanche Photodiode (APD) is similar to PIN diodes but operates at a higher reverse bias. A reverse bias at near breakdown voltage is applied to the avalanche photo diode which will cause incident light to produce electron-hole pairs i.e. charge carriers. These charge carriers will travel at their saturation velocity which is the highest achievable velocity that the electrons or holes can feasibly travel at. At saturation velocity these carriers will collide with other atoms and so new electron-hole pairs will be produced. This phenomena is known as impact ionisation. The process of impact ionisation also offers internal gain before the signal has even reached the amplifier which enables the detection of very weak optical fibre signals. This leads APD to be the most used form of photodiode in long-haul fibre optics communications.

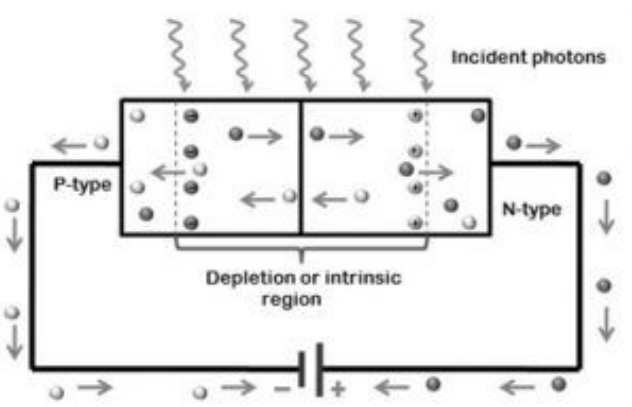

Figure 14: Graphic of Working Principle Behind Photodiodes [14]

Bit Error Rate

The Bit Error Rate (BER) is a measure of how reliable a communications system is and it is the primary metric by which the quality of fibre communications is measured. The formula for the BER is as follows,

$$\mathbf{BER} = \frac{\mathbf{Number\ of\ Bit\ Errors}}{\mathbf{Total\ Number\ of\ Bits\ Transmitted}}$$

A way of measuring the quality of data transmission is to investigate the qualities of the EYE diagram. An EYE diagram is a graphical tool use to evaluate the quality of a digital signal via time domain responses. This is done by overlaying the bit signals on top of each other to observe a distribution of how the bits are transmitted. The EYE diagram allows for insights into the jitter, noise, signal-to-noise ratio,rise-time and Q factor. The jitter is the variations in the timing of bit readings which quantifies the uncertainty as to when a signal will be received. Noise is the undesirable fluctuation which are superimposed onto a signal and can occur due to a variety of reason ranging from, thermal noise, background light, amplifier noise et cetera. The signal-to-noise ration is a measure of how distinct a signal is amidst noise and is defined by the equation,

$$\boxed{\mathbf{SNR}(dB) = 10log\left(\frac{P_{signal}}{P_{noise}}\right)}$$

The rise-time is the time taken for a signal to transition from low to high and is usually taken from 10% to 90% of the amplitude. A fater rise-time will result in sahrper edges in the EYE diagram and will correspond with better timing accuracy. The Q factor (or the Quality Factor) gives an insight to the signal quality by relating the BER to a Gaussian error function. The definition is as follows,

$$\boxed{Q = \frac{I_1 - I_0}{\sigma_1 + \sigma_0}}$$

where I_1 and I_0 are mean signal levels for bits "1" and "0" respectively and σ_1 and σ_0 are the standard deviation of their respective noise levels.

A Pseudo-Random Bit Stream (PRBS) is essential when analysing EYE diagrams and BER. A PRBS is a deterministic sequence of binary bits that mimic a truly random sequence, they are used to simulated real life data traffic in the optical channel.

Attenuation and Dispersion

A light signal travelling through an optical fibre is subject to a phenomenon known as attenuation. Attenuation represents the decrease in the amplitude of a signal, also known as transmission loss. It is measured in units of dB which is the logarithm of the ratio of the input power to the output power.

$$\boxed{\alpha_L = 10log(\frac{P_i}{P_o})}$$

Where

- α_L is attenuation coefficient dB,
- P is the power W,
- i and o are the initial and final values for the respective quantities

In this case the launch power is set to the basis power, which is half of the maximum output power. Some factors which contribute to attenuation are; Material Absorption, Fibre Bending, Linear and Nonlinear Scattering Loses as well as different types of Dispersion such as Chromatic, Material, Waveguide and Intermodal.

We can determine how dispersive the fibre is by calculating the time domain response, which is how an output of a signal change with time. We can determine what the time response is for the transmitter and receiver over a short distance, in this case 1 meter, determine the time response for the transmitter, receiver and fibre and deduce the time response due to solely the fibre. This can be calculated with the following equation,

$$\boxed{\tau_F = \sqrt{(\tau_S^2 - \tau_O^2)}}$$

where

- τ_F is the time response of the fibre
- τ_S is the time response of the entire system
- τ_O is the time response of the transmitter and receiver

This time response domain is related to the Bit Error Rate (BER) of the optical fibre which can been thought of as the probability that an encoded bit will be incorrectly measured, a 1 reads as a 0 and vice versa. We can use the measurements for τ_F to calculate what is called the Bandwidth Length Product. The term bandwidth–distance product (or bandwidth–length product) is often used in the context of optical fibre communications. It is usually defined as the product of the length of a fibre-optic link and its maximum signal bandwidth. [15]

An analogous method can also be used to determine the amount of material and intermodal dispersion with the equation,

$$\boxed{\tau_{R(tot)} = \sqrt{(\tau_{mat}^2 + \tau_{im}^2)}}$$

where

- $\tau_{R(tot)}$ is the total amount of dispersion
- τ_{mat} is the amount of material dispersion
- τ_{im} is amount of intermodal dispersion

The LASER is used to determine what the intermodal dispersion is because the linewidth is negligible so we can ignore the term which contributes to the material dispersion. The LED can be used to determine the material dispersion because the LED has a larger linewidth and it is now known what the intermodal dispersion is. The material dispersion parameter in the fibre at a wavelength λ can then be obtained from the following expression,

$$\boxed{D_{mat} = \frac{\tau_{mat}}{\Delta\lambda}}$$

where $\Delta\lambda$ is the spectral linewidth of the source. The intermodal dispersion parameter is determined by,

$$\boxed{D_{im} = \frac{\tau_{im}}{L}}$$

where L is the length of the optical fibre. The length can be calculated by taking the optical path length ($\Delta x = nL$) and the distance travel by light ($\Delta x = c\Delta t$) which gives us,

$$\boxed{L = \frac{c\Delta t}{n}}$$

Material absorption is one of the most prominent reasons that attenuation occurs in an optical fibre. Due to the defects in the material distribution on the fibre, the transmitted light is dissipated as heat out of the cladding which results in signal loss. Material absorption can be categorised into two different forms; intrinsic and extrinsic. At shorter wavelengths, intrinsic absorption is more dominant, this is also known as ultra-violent absorption. This absorption is due to an interaction between SiO band and EM field of optical region that takes place. Extrinsic absorption is due to the metal ions which are deposited during thin layer deposition to increase the refractive index of the fibre.

Bending the fire will also result in a higher attenuation due to more of the light pulse transitioning into the cladding at the bend. However, the attenuation is negligible due to fibre bending is negligible in comparison to some other factors such as scattering and dispersion. When making kilometre long optical fibres it is mandatory to have joints at different intersections of the fibres. These joints come in two different forms; splices which are permanent and connectors which can be added or removed to an optical channel. We examined the various different insertion losses for different components

of the apparatus that we have used. Overall connector losses typically only add an attenuation in a range of 0.5 dB and 1.0 dB.

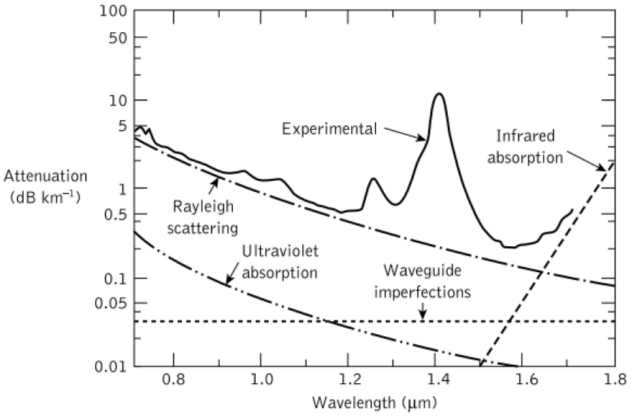

Figure 15: Attenuation graph [16]

Linear and Nonlinear Scattering

Scattering losses play a major part in the propagation of EM waves in optical fibres and there are various different types. Scattering occurs due to the non-uniformities and density fluctuations in fibre optic cable which cause a straight line path of light rays to deviate. Once this happens, some optical power from one mode is then transferred to another mode and this transfer of power takes place through the radiation mode (the mode which is one order higher than the highest mode achievable in the fibre). In the case of multimode fibres, there is a particularly higher level compositional fluctuations which lead to more scattering occurring. There is linear scattering which is described by Rayleigh scattering and Mie scattering, and there is nonlinear scattering which arise as stimulated Brillouin scattering and stimulated Raman scattering. Scattering along with intermodal dispersion result in a higher Bit error rate which will be seen later in the results and analysis section.

Rayleigh scattering is phenomenon that was proposed by Lord Rayleigh in 1871 in his paper "XV. On the light from the sky, its polarization and colour" [17]. In the paper Rayleigh verifies that the amount of scattering that light undergoes whenever collide with particles is λ^{-4} and that the scattering occurs in all directions. Glass fibres are amorphous materials, meaning that they have fluctuations in density and refractive index, the energy losses in glass fibres are given by the Rayleigh coefficient [**?**]:

$$\boxed{\alpha_{\text{scat}} = \frac{8\pi^3}{3\lambda^4} n^8 P^2 k T_{\text{f}} \beta}$$

Where

- n is the refractive index
- P is the photoelastic coefficient of the glass
- k is Boltzmann's constant
- β is the isothermal compressibility
- T_f is a fictive temperature, representing the temperature at which the density fluctuations are "frozen" in the material.

Mie scattering also plays a vital role in the attenuation of signals and is caused by atoms or molecules which are comparable in size with the wavelength. Mie scattering only occurs in the forward direction and the reasons for this type of scattering happening are similar to that of Rayleigh scattering, due to the imperfections of the design of the fibre. This form of scattering can be mitigated by removing the imperfections of the fibre and increasing the refractive index between the core and cladding.

Nonlinear scattering is similar in principle to linear scattering with the difference being that once power has transferred from one mode to another there is also a change in frequency. Nonlinear scattering produced optical gain but there will be a shift in frequency and this shift will result in a loss of signal, nonlinear scattering arises in nonlinear optics where the polarisation vector $\vec{P}$ in the dielectric does not change linearly with a change in the electric field $\vec{E}$ and the susceptibility of the the medium is expressed as a Taylor Series.

$$P = P_0 + \varepsilon_0 \chi^{(1)} E + \varepsilon_0 \chi^{(2)} E^2 + \varepsilon_0 \chi^{(3)} E^3 + \cdots$$

Nonlinear scattering ensues in two ways in fibres, via stimulated Brillouin scattering and stimulated Raman scattering, the stimulation is coming from a pump LASER. To better understand the nature of nonlinear scattering it is crucial to realise that once a wave of light is propagating at very high speed through the fibre the light causes ions in the medium to vibrate. The oscillations result in a quasiparticle known as phonons, and similar to photons, they represent the quantisation of acoustic waves in the medium just like how photons represent the quantisation of light energy. Phonons come in two different types; acoustic phonons and optical phonons. Acoustic phonons occur whenever the ions are oscillating in-phase with one another and optical phonons occur whenever the ions are oscillating out-of-phase with one another. The displacement of the ions in the medium causes a phenomenon known as electrostriction, which is the change in the medium's shape once it is subjected to an electric field, the dielectric will tend to elongate due to the oscillating ions. The positive ions in the material will accelerate in the direction of the field and the negative ions will accelerate in the opposite direction of the field.

The fundamental nature of the Brillouin interaction can be described as follows: interference between optical modes of a waveguide generates a pressure, or a force density, on the material, arising from radiation pressure or electrostriction. This pressure then excites an acoustic wave, provided that energy and momentum are conserved in the interaction. In turn, the strains of the acoustic field change the dielectric properties of the medium and perturb its boundaries, effectively creating a grating that scatters light from one optical mode to another. [18] Once the light pulse is transferred to

another mode there will be a frequency shift which is known as the Brillouin Frequency Shift:

$$\boxed{\nu_B = \frac{2n\nu_a}{\lambda}}$$

Where:

- n is the refractive index
- ν_a is the frequency of the acoustic wave
- λ is the vacuum wavelength

(For Brillouin scattering in fibres, the effective refractive index must be used.) [19]

Another form of nonlinear scattering is stimulated Raman scattering and the only difference between Raman scattering and Brillouin scattering is that the incident photons interact with the optical phonons as opposed to the acoustic phonons. Raman scattering can also incite a physical phenomenon known as Raman gain, wherein the optical power is increased due to the interaction between a phonon and a photon. This can only occur if the vibrational energy of the medium is at its ground state, otherwise a wave will be produced (known as Stokes wave) which will have an angular frequency which is equal to the difference of the angular frequency of the photon and the phonon. This is the main premise behind Raman Amplification which reduces the effect of pulse spreading by creating another signal photon that continues to propagate through the fibre.

WDM

Wavelength Division Multiplexing (WDM) is a method of multiplexing multiple optical carrier signals onto a single optical fibre by using different wavelengths (or frequencies) of light to carry separate data streams simultaneously. WDM allows a single fibre to transmit multiple independent signals in parallel, massively increasing its data-carrying capacity without laying more fibres. Each data stream is modulated onto a distinct optical wavelength using individual laser sources. These signals are then combined (multiplexed) and transmitted through a single fibre. At the receiving end, they are separated (demultiplexed) using wavelength-selective components and sent to their respective receivers. There are different types of WDM, there is Course WDM (CWDM) and Dense WDM (DWDM). CWDM has a wider channel spacing of about 20nm and is cheaper and simpler than DWDN because there is no need for rigorous temperature control. Although, CWDM does not allow for data transfers as high as DWDM does. This is because DWDM allows for more narrow channel spacing of around 0.8nm. DWDM typically operates in the C-Band (1530nm - 1565nm) and L-Band (1565 - 1625nm) and allows for up to 160 channels. WDM systems consist of several different components which include; DFB LASERs, multiplexers (MUX), demultiplexers (DEMUX), optical amplifiers (EDFAs), optical add-drop multiplexers, wavelength filters such as Fibre Bragg gratings and variable optical Attenuators.

Optical Amplifiers

Optical amplifiers are used to amplify an optical signal that is propagating through a fibre channel. These signals do not need to be converted back into their preliminary electrical signal, they can easily be amplified as electromagnetic radiation. Optical amplifiers can be placed anywhere along the optical path and are bidirectional, they also allow multiple signals to be amplified at once. Optical amplifiers can be implemented into the optical channel in many different ways. They can be implemented into the optical channel via in-line amplifiers, preamplifiers, transmission boosters and signal boosters. In-line amplifiers, as well as booster amplifiers are used to increase the transmission distance of a signal, preamplifiers are used to increase the sensitivity of the receiver and signal boosters amplifiers (LAN booster amplifiers) are used to distribute a signal to multiple receivers. Optical amplifiers can be categorised into three different types; Semiconductor Optical Amplifiers (SOA), Doped-Fibre Amplifiers (DFA) such as Erbium-Doped Fibre Amplifiers, and Raman Amplifiers.

Semiconductor and Doped-Fibre Optical Amplifiers operate under stimulated emission, similar to LASERs. SOAs are essentially an InGaAsP LASER which does not undergo the Purcell effect. For a conventional LASER diode there is a gain medium which is encapsulated in a resonator cavity structure, for SOAs the structure is nearly identical with the exception that the mirrors in the resonator cavity have a relatively lower reflectivity. The lower reflectivity of the amplifiers does not allow for lasing to take place, this is to ensure that the amplifiers themselves do not generate an optical signal but only provide energy to allow optical gain to occur for the propagating signal. The working premise behind an SOA or DFA is that a "pump" LASER is used to provide energy to the electrons within an active medium so that they become excited and population inversion occurs. Once this has been achieved, the incoming signal will induce stimulated emission and generate photons with the same wavelength. This will result in an optically amplified signal.

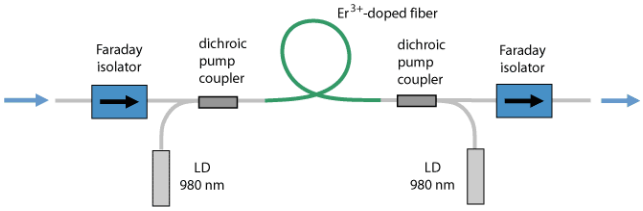

Figure 16: Schematic setup of a simple erbium-doped fiber amplifier [20]

A particularly ubiquitous form of DFA is Erbium-Doped Fibre Amplification (EDFA). This method entails creating an erbium-doped fibre which is spliced into the optical fibre channel and a pump LASER being incident on it at 980nm, as shown in Figure 11. Erbium is used in particular because it has quantum levels which allow for stimulated emission to produce photons which have a wavelength in the 1530nm - 1580nm range. [21] Figure 12 shows how electrons are

excited to a pump band, which then quickly decay to the metastable band. This metastable band becomes densely populated and allows for stimulated emission to occur from the signal photons and produce coherent photons with gain.

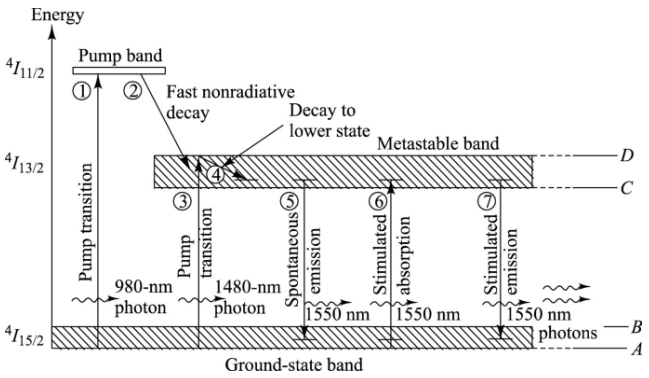

Figure 17: Energy Level Diagram for EDFA [22]

Raman Amplifiers operate under a different physical process which doesn't require population inversion and instead exploits Raman Scattering. This type of amplification does not require a doped fibre and is easier to implement into an optical channel than SOAs. The main premise behind Raman Amplifiers is that an incident photon will excite electrons in the fibre and the electrons will quickly decay back into the ground state. Once the electron has decayed back into the ground state, there will be a photon released which has a lower energy and a phonon with the difference in energy will also be released. The shift in wavelength from the incident photon to the scattered photon is known as Stokes shift and the exact Stokes shift is different depending on the material that is used in the optical fibre.

Optical Amplifiers are some of the most important optical components in fibre communications.

Optical Components

There are a variety of optical components that are used to streamline the efficacy of optical fibre communications. The particular components which were investigated included the Fused Biconical Taper (FBT) Coupler, the Isolator, the Circulator, Optical Add-Drop Multiplexers (OADM), the Variable Optical Attenuator (VOA) and the Bragg Grating Fibre. All of these components have their characteristics and operate in different ways by utilising different physical concepts.

We will first discuss the properties of the FBT coupler because of how most fibre optic components are based on the principles of couplers. Couplers allow the transfer of power form one fibre to another and this is done through evanescent waves. Two fibres are twisted together and fused under heat treatment so that their cores are as close as possible. The length for which this proximity is consistent is known as the coupling length which dictates the coupling ratio, the FBT coupler which was used throughout the experiments was the 50/50 ratio coupler.

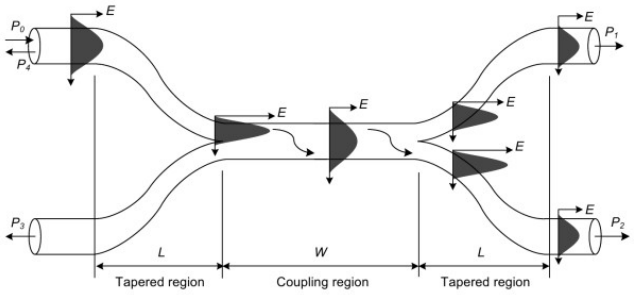

Figure 18: Polarisation Independent Isolator [23]

There are certain parameters which determine whether or not an FBT coupler is of good quality, meaning if it does what it is designed to do. These parameters are; the splitting ratio, the insertion loss, the excess loss and the return loss (also known as the cross-talk). The splitting ratio is the percentage of output power which is coupled, the insertion loss is the particular port-to-port loss, the excess loss is the ratio of input power to the total output power and the return loss is the ratio of the reflected signal to the input signal. All of these losses are in terms of dB.

$$\textbf{Splitting Ratio} = \left(\frac{P_2}{P_1 + P_2}\right) \times 100$$

$$\textbf{Excess Loss} = 10log\left(\frac{P_0}{P_1 + P_2}\right)$$

$$\textbf{Insertion Loss} = 10log\left(\frac{P_i}{P_j}\right)$$

$$\textbf{Return Loss} = 10log\left(\frac{P_4}{P_0}\right)$$

We will now discuss the use of the optical isolator. An isolator is used to mitigate the interference and temperature differences that might occur when a signal is travelling through the optical channel, this is done by ensuring the signal travels in only one direction. The optical isolator exploits birefringence with the Faraday Effect to do so. Birefringence occurs whenever electromagnetic radiation passes through an anisotropic medium which means that the refractive index of the material depends on the polarisation of the electromagnetic wave, this results in the different components of the wave being separated in the medium. The Faraday Effect is where the wave becomes circularly polarised when in the presence of a magnetic field according to the following equation:

$$\boxed{\beta = \nu B d}$$

where

- ν is the Verdet constant of the material of which the rotator is made
- d is the length of the rotator
- B is the magnitude of the magnetic field

The blue ray in Figure 13 represents the incident ray of light and the red ray represents the reflected ray of light and shows how the reflected ray is not transmitted.

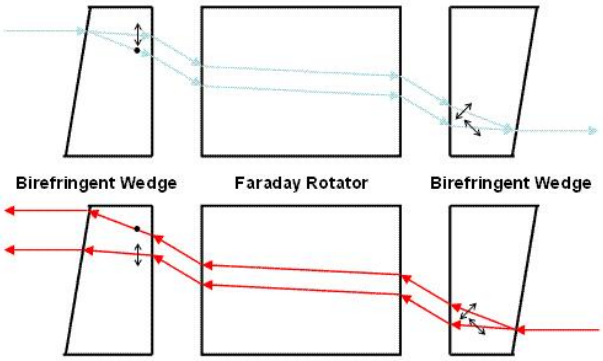

Figure 19: Polarisation Independent Isolator [23]

Optical Circulators also achieve a similar idea however circulators can be used to also split a signal as well as making it travel in a single direction. The optical circulator is used in conjunction with the Bragg grating fibre for temperature sensing. Light enter at port 1 and is passed through a polarisation beam splitter, can also be a birefringent element which separates the ordinary and extra-ordinary rays. Similar to the optical isolator, the beam will pass through a Faraday rotator, rotating the polarised state by 45 degrees. The signal enter port 2 will undergo circular polarisation once again which aligns the beam into a new state, ensuring it is directed to port 3.

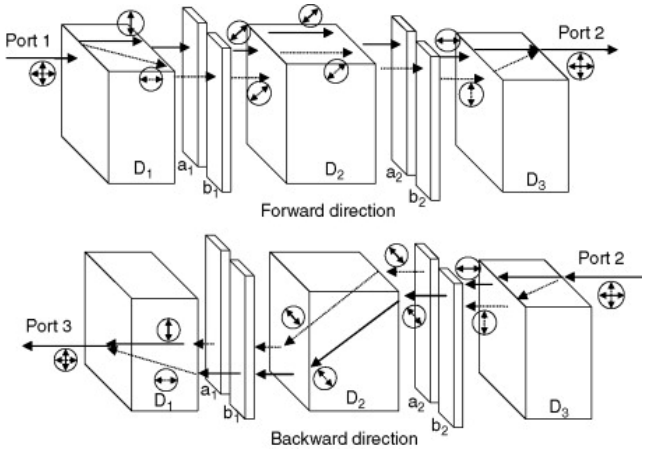

Figure 20: Schematic for Optical Circulator [24]

Optical Add-Drop Multiplexers is a device which allows for individual signals to be added or dropped from an optical channel. This is done by allowing specific wavelengths to pass through and others to be reflected, they are highly important in WDM. The OADM works in conjunction with the fibre Bragg grating in the experiment to simulate an optical signal being dropped and added to the channel. In the case of dropping a wavelength, the setups begins with a multiplexed input signal entering port 1 of a circulator. Port 2 of the circulator is connected to the FBG which is tuned to only allow certain a wavelength to be reflected while the others are passed unaffected. The reflected wavelength is routed through the circulator and dropped from the channel by connecting the circulator to the reflect port of the OADM. To add a signal we essentially go in reverse wherein the added signal will instead be reflected into the circulator and pass through the FBG.

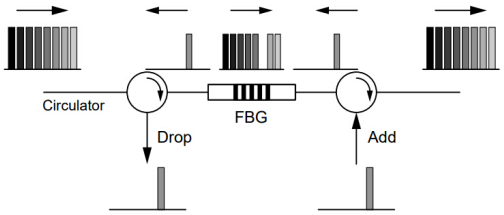

Figure 21: Schematic for Optical Circulator [24]

A Variable Optical Attenuator (VOA) is a tunable optical device which was used in experiments to simulate even longer stretches of optical fibre of up to 100km by inducing a power loss. They are particularly useful for power control to test performance. VOAs can be implemented via several different mechanisms, either mechanically, electrically or thermally. It may be just as simple as including an air gap to fabricate a loss of power.

The Fibre Bragg grating reflected a certain wavelength and allows others to pass in a multiplexed signal. This is done by taking a short segment of core within an optical fibre where the refractive index has been periodically modified along the axis of the fibre. This periodic modulation reflected the so-called Bragg-Wavelength and allows other wavelengths to pass unaffected. The fundamental principle behind an FBG relies on the concept of Bragg reflection which starts with light propagating through the fibre encounters the periodic variations in the refractive index and at a specific wavelength (the Bragg wavelength), reflected signals from each refractive index variation are constructively interfered, creating a strong reflected signal. All other wavelengths experience destructive interference and thus pass through the grating without significant reflection. The Bragg Wavelength is given by,

$$\lambda_B = 2n_{eff}\Lambda$$

where λ_B is the Bragg wavelength, n_{eff} is the effective refractive index of the fibre core and Λ is the grating period (the distance between each change in refractive index).

These are some of the most important components in industry and used frequently to enable WDM and DWDM.

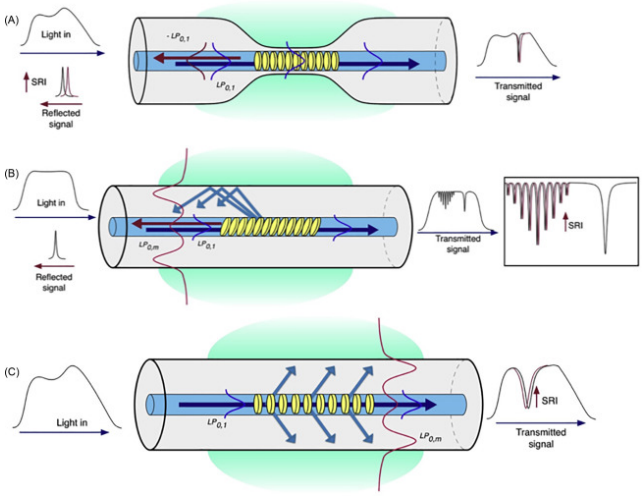

Figure 22: Schematic for Optical Circulator [25]

Results and Analysis

The difference in the characteristics of the LASER diode and the LED are shown in Figure 25. LED has a clear linear relationship from zero whereas the current must be above the threshold for the LASER to operate. Once the drive current is higher than the threshold it is clear to see that the output power for the LASER is exceptionally greater due to the coherence of the light being emitted.

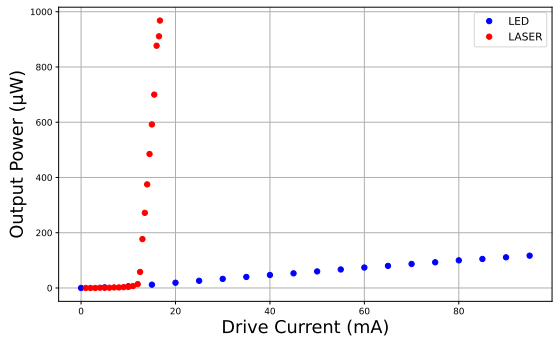

Figure 23: LASER and LED Characteristic Through a Patchcord

We can see form Figure 26 how the output power changes with an increase in the length of the optical fibre. As the fibre becomes longer, the output power at the receiver becomes lowers, this is due to attenuation and dispersion. The relationship for LED is similar with the exception that the absolute increase in output power is significantly less, on the order of about $100\mu W$. Figure 27 to Figure 30 all show how the temperature influences the threshold current at different lengths of fibre for a LASER. In Figure 27 we can see that the LASER threshold current is approximately 6.5-7 mA and the maximum output power reaches 3.4mW at a drive current of 89.5mA. The Voltage also steadily rises and is around 1.4V at 89.5mA. In Figure 28 we can see that the threshold current shifts to about 8mA, indicating that more current is required to begin lasing and the maximum power out only reaches 3.0mW. The increase in threshold temperature is due to the charge carrier leakage and the maximum power output decreases because the current is contributing more to thermal losses. The voltage does not change in either of the Figures. The effect is more exaggerated in Figure 29 and 30 and they show a clear nonlinear relationship in their transitions. In summary, the power drops, the threshold rises and the voltage shift with heat so it is important to maintain thermal stability within the optical fibres.

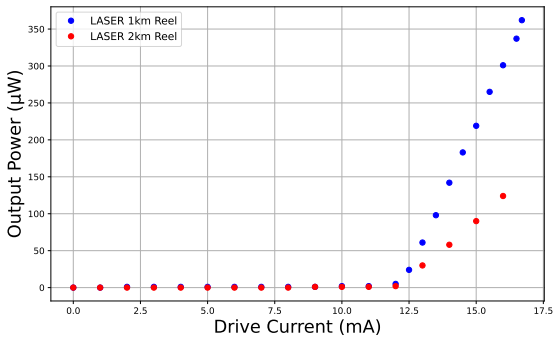

Figure 24: Drive current of LASER in different Length of Optical Fibre

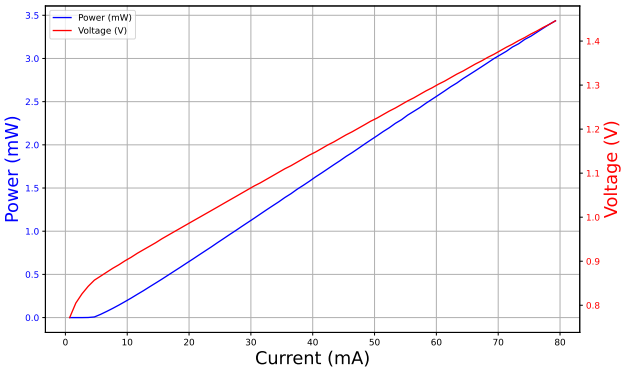

Figure 25: Current, Power and Voltage of LASER at $10°C$ through Patchchord

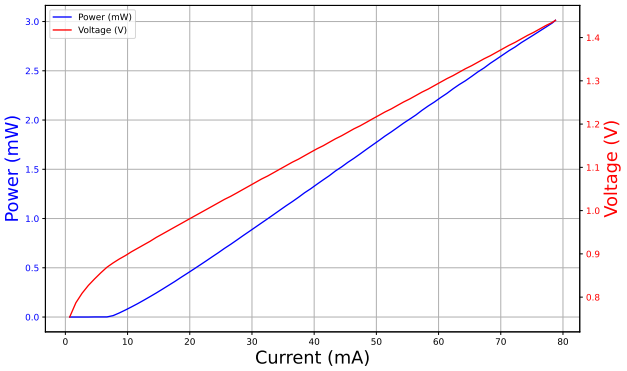

Figure 26: Current, Power and Voltage of LASER at $40°C$ through Patchchord

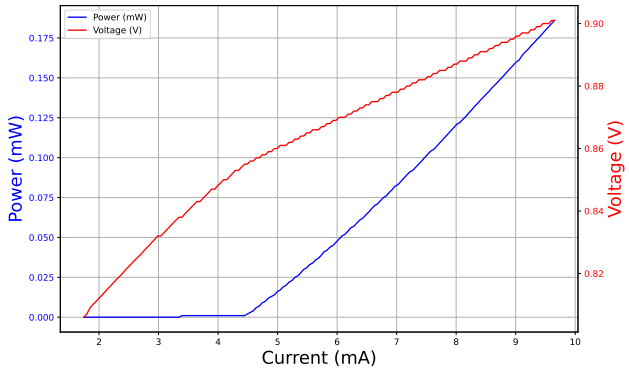

Figure 27: Current, Power and Voltage of LASER at $10°C$ through 5km fibre

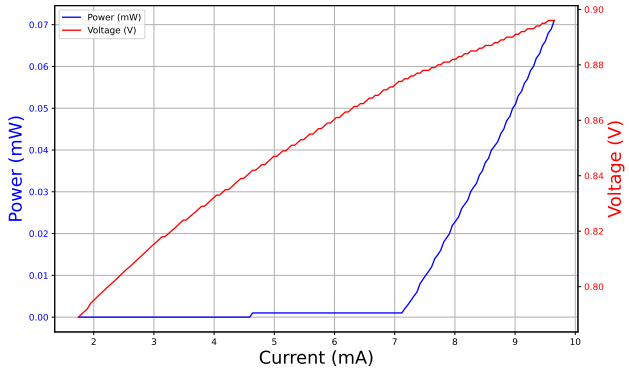

Figure 28: Current, Power and Voltage of LASER at $40°C$ through 5km fibre

The Bandwidth Length Product (BLP) and Bit Rate Length Product (BRL) will allow us to determine the contribution of intermodal and material dispersion that occurs in the different arrangements of fibre. Higher BLP corresponds to a higher capacity for signals to travel over long distances and BRL describes the maximum digital bit rate that a fibre can support over a given distance. Table 2 and 3 show how the dispersion from the LASER and LED respectively, the BLP is measured in $MHz \cdot km$, BRL is measure in $Mbps$, material and intermodal dispersion are measured in $ps/nm \cdot km$. It is important to note that reel 2 is approximately twice the length of reel one.

These set of results also confirm that it is best for a LASER to be used within a a single-mode fibre to mitigate the amount of intermodal dispersion because the amount of intermodal dispersion contributes a lot more than the amount of material dispersion.

Table 2: Table Showing Dispersion using LASER

Optical Fibre Reels	Bandwidth Length Product	Bit Rate Length Product	Intermodal Dispersion
Reel 1	30.2	40.4	6183 ± 144
Reel 2	490	76.7	3300 ± 116
Combined Fibre	463	106.9	3400 ± 199

Table 3: Table Showing Dispersion using LED

Optical Fibre Reels	Bandwidth Length Product	Bit Rate Length Product	Material Dispersion
Reel 1	0.09	40	32 ± 5
Reel 2	0.07	66	66 ± 6
Combined Fibre	0.06	81	67 ± 19

In Figure 31 and 32 the results are as expected, the BER increases and the Q-factor decreases with both increasing bit rate and fibre length. These trends are symptomatic of dispersion-induced degradation, where pulse broadening and inter-symbol interference reduce signal fidelity. The system performs robustly at short distances (1–2 km), but at longer distances (4–5 km), the Q-factor falls below acceptable limits and BER becomes unacceptably high, particularly beyond 20 Mb/s. These results underscore the importance of dispersion management and bit rate-distance optimization in digital optical communication systems.

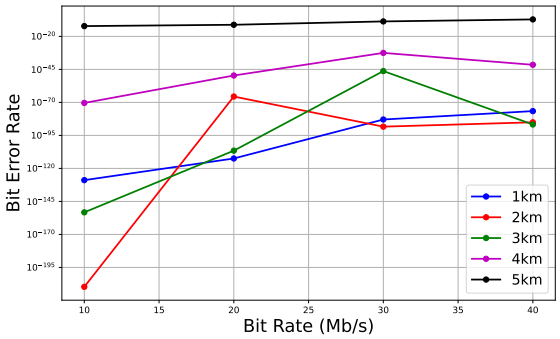

Figure 29: Bit Error Rate against the Bit Rate for a LASER Propagating through Different Lengths of Fibre

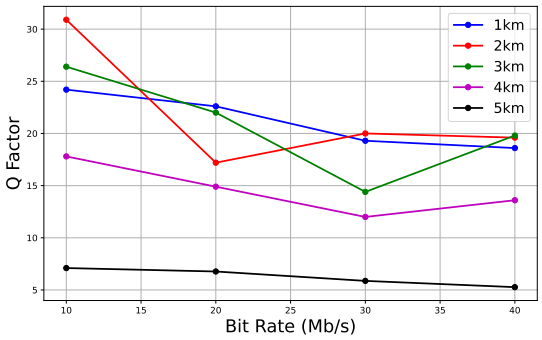

Figure 30: Q Factor against the Bit Rate for a LASER Propagating through Different Lengths of Fibre

Figure 33 what a good quality signal would be expected to look like. The very large signal separation of 50V between a "1" and "0" bit leave a lot of room for noise to occur, this signal is of high quality because of the short distance it travels. There is also an exceptionally high Q factor of 34.8 and the BER is essentially zero for practical terms at 7.9×10^{-266}. The histogram shows a tall and skinny bell curve which correlates to minimal jitter. Figure 34 on the other hand

is what we would typically see in practice. The voltage between the bits is now 0.4V and the histograms are wider which corresponds to a higher risk of overlap and a bit error occuring. The Q factor is 7.1 which is still acceptable but no where near the quality of Figure 33. The BER is $\approx 10^{-13}$ which again is acceptable but not ideal for long-haul transmissions. In summary, he Q-factor histograms reveal a clear relationship between transmission distance and signal quality. At 1m, the system exhibits an excellent Q-factor of 34.8 with near-zero BER, indicating exceptional SNR and negligible distortion. However, for the longer reel setup, the Q-factor falls to 7.1 and BER rises to 6.1×10^{-13}, demonstrating the effects of attenuation, dispersion, and noise accumulation. The voltage histogram broadening further confirms increased signal jitter and reduced noise margins.

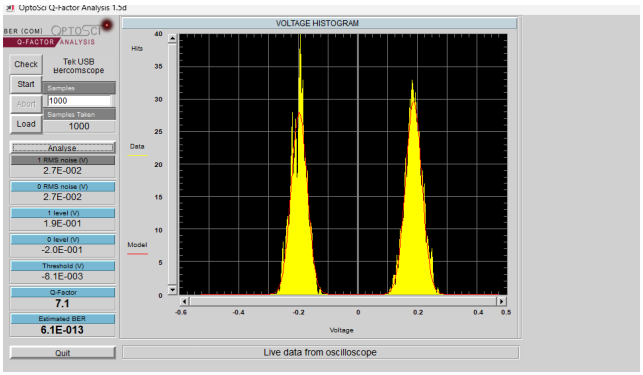

Figure 32: Optosci Software used to measure the Q factor of Signal Propagating through 5km of Fibre Reel via LASER at 10Mbps

The software that is used in Figure 33 and 34 is used to measure the distribution of the the bits which are received at different lengths of fibre using LASER. We can see the Gaussian distribution of the registered bits which is then used to approximate the mean and standard deviation and calculate the Q factor. This calculation was all done within the Optosci Q-factor Analysis Software but could be done by hand by exporting the readings in a csv file and carrying out statistical analysis to determine the uncertainty of the Q factor but for the sake of brevity and continuing with other experiments, this was decidedly left out but would be something to go back and do if the opportunity was given.

Figure 35, 36 and 37 show the EYE diagrams were acquired to visualise signal quality under varying transmission conditions. The 1m laser link at 10Mbps showed a wide-open eye, indicating negligible noise or jitter, and optimal timing margins. This image indicates what a clear signal would look like on an oscilloscope. In contrast, the 5km laser link at 40Mbps exhibited significant eye closure, consistent with dispersion and inter-symbol interference, reducing SNR and increasing BER. The LED source over 5km at 10Mbps produced a partially open eye, degraded by broader spectral output and reduced modulation speed, but still within acceptable limits for low-speed data. The LASER clear outperforms the LED when it comes to long-haul transmission at high data rates.

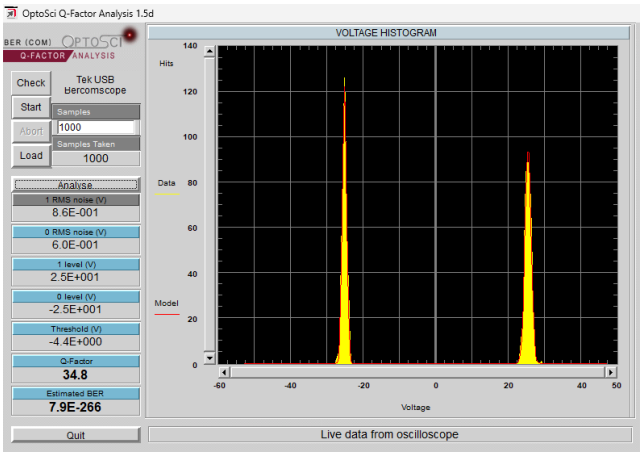

Figure 31: Optosci Software used to measure the Q factor of Signal Propagating through 1m Patchchord via LASER at 10Mbps

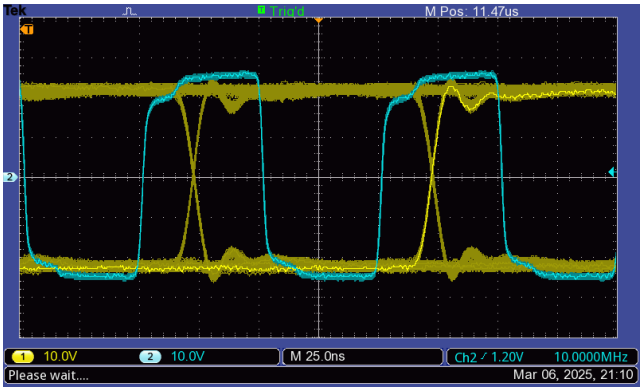

Figure 33: EYE Diagram for LASER travelling through 1m Patchchord at 10Mbps

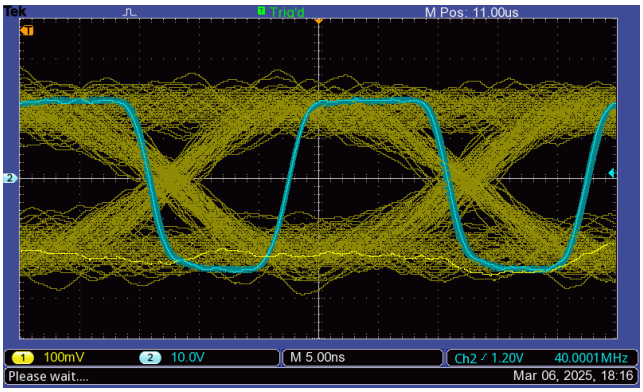

Figure 34: EYE Diagram for LASER travelling through 5km Fibre at 40Mbps

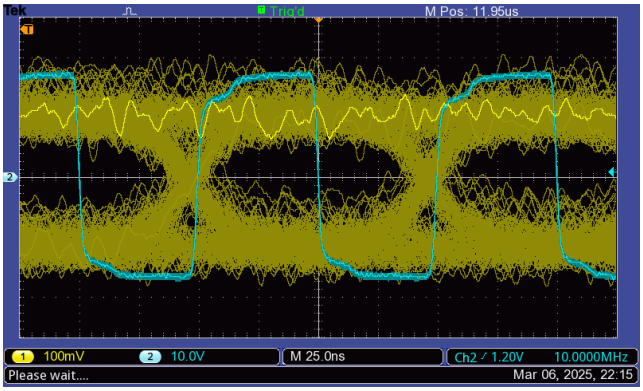

Figure 35: EYE Diagram for LED travelling through 5km Fibre at 10Mbps

The characteristics of the FBT Coupler and the ITU35 module are shown in Figure 38 and 39 respectively. Figure 38 shows that the operational wavelength of the coupler is between 1549.75nm and 1550.50nm. This the cross over region where the upper and lower channels intersect which indicates a balanced splitting near the central wavelength around 1550nm. Maximum coupling occurs around the 1550nm mark, showing that it operates properly at this wavelength.

We can see from Figure 38 that the splitting ration is roughly 50/50 around 1550nm, the bandwidth of the coupler is 2nm, there is low insertion loss near the central wavelength and that the coupler is highly wavelength dependent.

The spectral transmission shown in Figure 39 is that of the ITU35 channel and we can see that the central wavelength is approximately 1549.32nm. The passband is very narrow which is in line with the stand of ITU35 channels in industry, the passband is the two peaks on adjacent to the lowest trough at either side. The peak power approaches approximately -25dB, indicating a high transmission efficiency. There is a steeper roll as the signal increases in wavelength in comparison to when it decreases in wavelength. This could indicate a slight defect in the signal selectivity this channel.

Overall, the FBT coupler demonstrated a symmetric splitting behaviour near 1550 nm, confirming its 50/50 coupling ratio. This makes it ideal for equal-power distribution in passive optical networks. On the other hand, the ITU35 DWDM module showed a sharp, narrow transmission peak centred at 1549.32 nm with excellent channel isolation, validating its role as a highly selective wavelength filter in dense WDM systems.

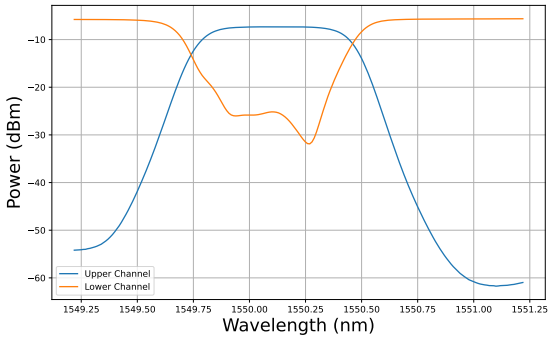

Figure 36: Characteristic of FBT Coupler

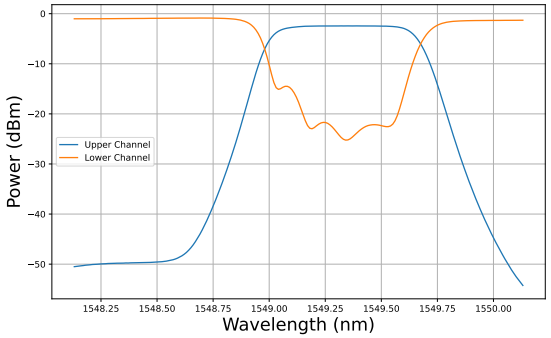

Figure 37: Characteristic of ITU35 Module

The spectral response of the Fibre Bragg Grating was measured at $10.2°C$ and $40.1°C$ in Figure 40 and 41 respectively show a clear shift in their peaks. Figure 40 shows a peak at 1549.90nm and Figure 41 shows a peak at 1550.2nm. Both the upper and lower channel powers peak symmetrically about this point and the power peak reaches roughly 30dBm for Figure 40 and 41. The results clearly show a redshift in the Bragg reflection peak of approximately 0.3 nm, consistent with theoretical predictions based on thermal expansion of the periodic cores. This confirms the FBG's sensitivity to temperature, making it a viable component for distributed temperature sensing in fibre optic systems.

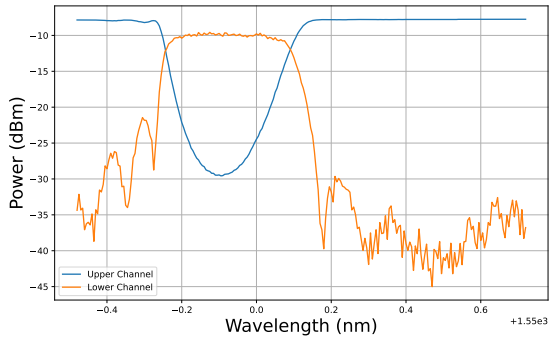

Figure 38: Characteristic of Bragg Grating at 10.2°

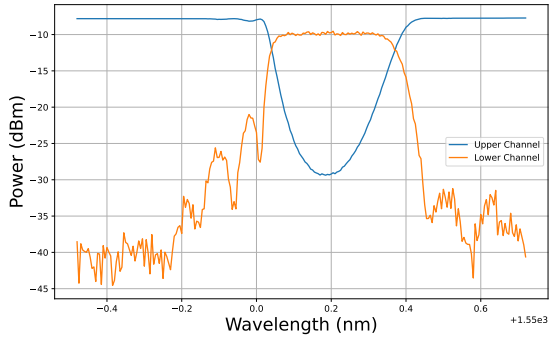

Figure 39: Characteristic of Bragg Grating at 40.1°

Figure 42 to 44 show the transmission of a signal through the DWDM module at different lengths to determine whether or not the OADM is capable of fully filtering out different wavelengths. To start with, Figure 42 shows a peak transmission level in the upper channel centred at roughly at 1550.12nm which is consistent with the ITU34 channel. The wavelength difference between each channel in DWDM is approximately 0.8nm and the peak of the upper channel falls within 0.8nm of the central channel wavelength. Both Figure 43 and 44 show show the same concept of filter selectivity but the overall output power is weaker because of the increase in length of the optical fibre. Figure 45 confirms the selectivity of the ITU35 channel. The passband is clearly centred around the 1549.32nm which is characteristic of the ITU35 channel. The lower channel also exhibits steep roll-off on both sides which again indicate great spectral selectivity. The channel isolation can also be seen with how the power drops from ≈4dBm to below 22dBm. The peak transmission is around 4dBm which indicates some insertion loss but still within acceptable limits. This figure confirms that the DWDM filter module targeting ITU Channel 34 is well-aligned and highly selective. The Lower Channel shows a passband centred at 1549.32 nm with a 0.3 nm width and steep roll-off, ensuring strong isolation from adjacent channels. The flat, high-power Upper Channel suggests it is a pass-through or monitoring port. Overall, this filter is suitable for high-density WDM systems requiring precise wavelength control and minimal crosstalk.

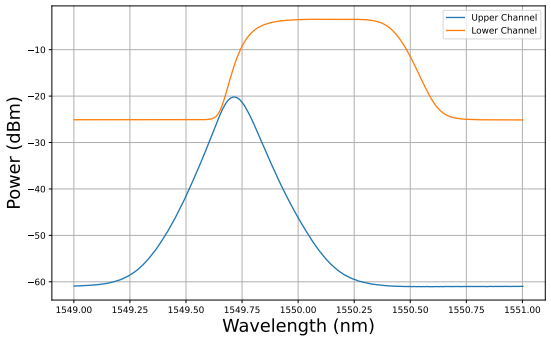

Figure 40: Characteristic of 1550.12nm Signal through 1m Patchchord

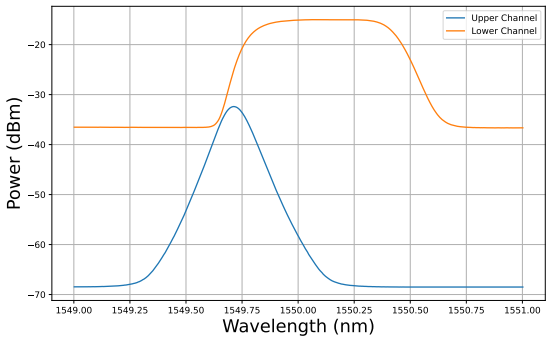

Figure 41: Characteristic of 1550.12nm Signal through 4km Fibre

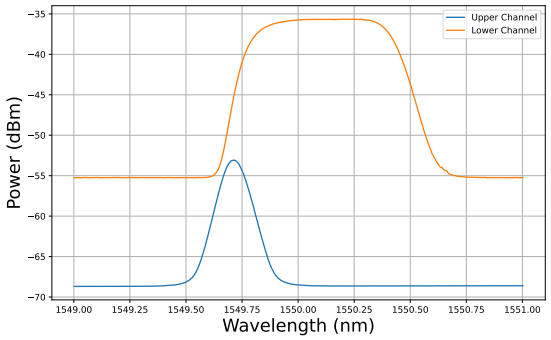

Figure 42: Characteristic of 1550.12nm Signal through 100km Fibre

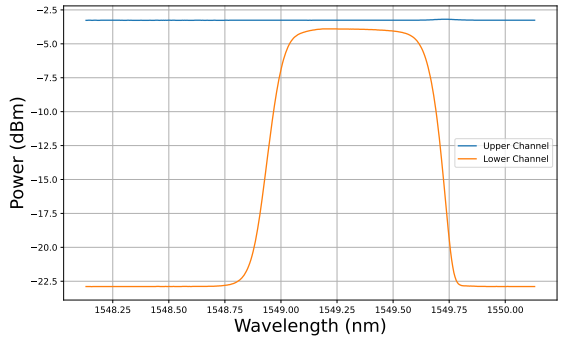

Figure 43: Transmission of 1550.12nm Wavelength through a ITU35 Channel

Conclusion

This investigation has explored the fundamental and advanced performance characteristics of optical waveguides and fibre optic components, with a focus on signal transmission quality, wavelength-dependent filtering, and the influence of system variables such as temperature, fibre length, bit rate, and source type. Experimental results confirmed the theoretical behaviour of light in guided media. Through Snell's law verification and reflection/refraction studies, core principles such as total internal reflection and guided mode propagation were validated. The performance of laser and LED sources was evaluated under varying conditions, revealing that laser diodes offer higher output power, better spectral purity, and sharper eye diagrams — especially over short distances — while LEDs suffer from broader spectra and increased dispersion over long fibres. Q-factor and BER analyses quantitatively demonstrated the degradation in signal quality with increasing fibre length and data rate. At short distances (1m), Q-factors exceeded 30 with BER values effectively zero, indicating near-perfect transmission. In contrast, transmission over 4–5km at higher bit rates (e.g., 40Mbps) resulted in substantial Q-factor reductions and increased BER, primarily due to inter-symbol interference and dispersion.The eye diagrams reinforced these findings visually, showing open, well-defined eyes at short distances and low bit rates, and closed, noisy eyes in longer, higher-speed scenarios. These results underscore the importance of balancing transmission rate and fibre length to maintain acceptable BER.Wavelength-dependent behaviours were characterised using Fibre Bragg Gratings (FBGs) and DWDM modules. The FBG responses confirmed the expected thermal shift in Bragg wavelength (0.25nm for a 30°C temperature rise), demonstrating their potential in precision sensing. The DWDM filter modules exhibited strong wavelength selectivity and channel isolation, centred on ITU-specified wavelengths such as 1549.32 nm (Channel 34) and 1550.12 nm (Channel 35), with passband widths consistent with 100 GHz spacing. The effect of optical attenuation was examined using a Variable Optical Attenuator (VOA), where the introduction of 25dB loss dramatically reduced power levels while preserving spectral shape — highlighting the VOA's use in system power balancing and receiver stress testing.

In conclusion, the experimental work has successfully demonstrated key operational features of fibre optic systems, from simple geometric optics to advanced digital performance metrics. The results align closely with theoretical expectations and provide valuable insight into the trade-offs and design considerations required for real-world optical communication networks

References

[1] L. A. Ngiejungbwen, H. Hamdaoui, and M.-Y. Chen, "Polymer optical fiber and fiber bragg grating sensors for biomedical engineering applications: A comprehensive review," *Optics & Laser Technology*, vol. 170, p. 110187, 2024. [Online]. Available: https://www.sciencedirect.com/science/article/pii/S0030399223010800

[2] B. J. Puttnam, R. S. Luis, I. Phillips, M. Tan, A. Donodin, D. Pratiwi, L. Dallachiesa, Y. Huang, M. Mazur, N. K. Fontaine, H. Chen, D. Chung, V. Ho, D. Orsuti, B. Boriboon, G. Rademacher, L. Palmieri, R. Man, R. Ryf, D. T. Neilson, W. Forysiak, and H. Furukawa, "402 tb/s gmi data-rate oesclu-band transmission," in *2024 Optical Fiber Communications Conference and Exhibition (OFC)*, March 2024, pp. 1–3.

[3] D. J. Griffiths, *Introduction to Electrodynamics*, 4th ed. Cambridge University Press, 2017.

[4] T. Bauer, "Optical materials — plastics," in *Encyclopedia of Modern Optics*, R. D. Guenther, Ed. Oxford: Elsevier, 2005, pp. 480–488. [Online]. Available: https://www.sciencedirect.com/science/article/pii/B0123693950008654

[5] B. Saleh and M. Teich, *Fundamentals of Photonics*, ser. Wiley Series in Pure and Applied Optics. Wiley, 2019. [Online]. Available: https://books.google.co.uk/books?id=rcqKDwAAQBAJ

[6] T. H. Maiman, "Stimulated optical radiation in ruby," *nature*, vol. 187, no. 4736, pp. 493–494, 1960.

[7] K. C. Kao and G. A. Hockham, "Dielectric-fibre surface waveguides for optical frequencies," in *Proceedings of the Institution of Electrical Engineers*, vol. 113, no. 7. IET, 1966, pp. 1151–1158.

[8] Nobelprize.org. (2013) The Nobel Prize in Physics 2009. http://www.nobelprize.org/nobel_prizes/physics/laureates/2009/.

[9] G. Keiser and G. Keiser, *Fiber optic communication networks*. Springer, 2021.

[10] R. J. Mears, L. Reekie, I. Jauncey, and D. N. Payne, "Low-noise erbium-doped fibre amplifier operating at 1.54 μm," *Electronics Letters*, vol. 23, no. 19, pp. 1026–1028, 1987.

[11] L. Gong, Q. Zhao, H. Zhang, X.-Y. Hu, K. Huang, J.-M. Yang, and Y.-M. Li, "Optical orbital-angular-momentum-multiplexed data transmission under high scattering," *Light: Science & Applications*, vol. 8, no. 1, p. 27, 2019.

[12] W. Commons, "File:singlemode fibre structure.svg — wikimedia commons, the free media repository," 2020, [Online; accessed 31-March-2025]. [Online]. Available: https://commons.wikimedia.org/w/index.php?title=File:Singlemode_fibre_structure.svg&oldid=481305095

[13] W. Johnstone, B. Culshaw, D. Walsh, D. Moodie, and I. Mauchline, "Photonics laboratory experiments for modern technology-based courses," *Proceedings of the IEEE*, vol. 88, pp. 41 – 54, 02 2000.

[14] ElectronicsHub, "File:singlemode fibre structure.svg — wikimedia commons, the free media repository," 2020, [Online; accessed 07-April-2025]. [Online]. Available: https://www.electronicshub.org/photodiode-working-characteristics-applications/

[15]

[16] F. Aznar, S. Celma, and B. Calvo, *Optical Signal Transmission*. New York, NY: Springer New York, 2013, pp. 19–59. [Online]. Available: https://doi.org/10.1007/978-1-4614-3464-1_2

[17] J. S. and, "Xv. on the light from the sky, its polarization and colour," *The London, Edinburgh, and Dublin Philosophical Magazine and Journal of Science*, vol. 41, no. 271, pp. 107–120, 1871. [Online]. Available: https://doi.org/10.1080/14786447108640452

[18] C. Wolff, M. J. A. Smith, B. Stiller, and C. G. Poulton, "Brillouin scattering—theory and experiment: tutorial," *J. Opt. Soc. Am. B*, vol. 38, no. 4, pp. 1243–1269, Apr 2021. [Online]. Available: https://opg.optica.org/josab/abstract.cfm?URI=josab-38-4-1243

[19] R. Paschotta, "Brillouin scattering," RP Photonics Encyclopedia, 2008. [Online]. Available: https://www.rp-photonics.com/brillouin_scattering.html

[20] ——, "Erbium-doped fiber amplifiers," RP Photonics Encyclopedia, 2007, available online at https://www.rp-photonics.com/erbium_doped_fiber_amplifiers.html. [Online]. Available: https://www.rp-photonics.com/erbium_doped_fiber_amplifiers.html

[21] G. Khan, "Analytical method for gain in erbium doped fiber amplifier with pumb excited state absorption," *Optical Fiber Technology*, vol. 18, no. 6, pp. 421–424, 2012.

[22] G. Keiser, *Basics of Optical Amplifiers*. Singapore: Springer Singapore, 2021, pp. 437–475. [Online]. Available: https://doi.org/10.1007/978-981-33-4665-9_11

[23] W. Commons, "File:optical isolator.gif — wikimedia commons, the free media repository," 2020, [Online; accessed 10-April-2025]. [Online]. Available: https://commons.wikimedia.org/w/index.php?title=File:Optical_isolator.GIF&oldid=485286019

[24] R. Hui and M. O'Sullivan, "Chapter 3 - characterization of optical devices," in *Fiber Optic Measurement Techniques*, R. Hui and M. O'Sullivan, Eds. Boston: Academic Press, 2009, pp. 259–363. [Online]. Available: https://www.sciencedirect.com/science/article/pii/B9780123738653000033

[25] D. Tosi, "Fiber optic biosensors," in *Encyclopedia of Sensors and Biosensors (First Edition)*, first edition ed., R. Narayan, Ed. Oxford: Elsevier, 2023, pp. 142–157. [Online]. Available: https://www.sciencedirect.com/science/article/pii/B9780128225486000704